Available online at www.sciencedirect.com
ScienceDirect
Catalysis Today 126 (2007) 54–63
CATALYSIS TODAY
www.elsevier.com/locate/cattod

Distinct spatial changes of the catalyst structure inside a fixed-bed microreactor during the partial oxidation of methane over Rh/Al_2O_3

Stefan Hannemann [a], Jan-Dierk Grunwaldt [a,*], Niels van Vegten [a], Alfons Baiker [a], Pit Boye [b,1], Christian G. Schroer [b,1]

[a] *Institute of Chemical and Bioengineering, Department of Chemistry and Applied Biosciences, ETH Zurich, Hönggerberg, HCI, CH-8093 Zurich, Switzerland*
[b] *HASYLAB at DESY, Notkestrasse 85, D-22607 Hamburg, Germany*

Available online 25 September 2006

Abstract

During the catalytic partial oxidation (CPO) of methane to hydrogen and carbon monoxide distinct spatial changes of the catalyst structure in a microreactor containing a fixed-bed of 2.5 wt% Rh/Al_2O_3 were observed depending on temperature and space velocity. The variation of the catalyst structure along the catalyst bed was determined by X-ray absorption spectroscopy. In a first step the catalyst bed was scanned with a small X-ray beam. Then, more detailed information on the oxidation state of Rh along the catalyst bed was extracted by recording absorption images using a position sensitive X-ray camera. The studies were combined with on-line mass spectrometry providing information on the catalytic performance of the catalyst simultaneously.

Mainly oxidized Rh-particles were found below the ignition temperature (310 °C) of the partial oxidation of methane to hydrogen and carbon monoxide. Hardly any structural changes were observed when oxidation to water and carbon dioxide occurred, but strong variations over the catalyst bed were detected when the CPO-reaction started. In the entrance zone of the catalyst bed the rhodium species were mainly in oxidized state, whereas they were in metallic state towards the end of the catalyst bed. Usually, a steep gradient within less than 100 μm was observed. Furthermore, at higher temperature, a characteristic cone towards the inlet of the spectroscopic cell was observed. Upon temperature increase the gradient zone moved towards the inlet. The variation of the space velocity also resulted in a shift as well as a change in the shape of the profile.

Keywords: *In situ* X-ray absorption spectroscopy; Catalytic partial oxidation of methane; Rhodium catalysts; 2D-imaging; Spatially resolved XAS; Micro EXAFS; XANES

1. Introduction

In situ or *operando* spectroscopic studies are used to gain mechanistic insight into the structure and working mechanisms of heterogeneous catalysts [1–7]. Spectroscopic studies under reaction conditions are vital since the structure is often more dynamic than anticipated [8–10]. However, only little attention has been paid to changes in the solid catalyst on a microscale up to now [11–18]. Usually, the *in situ* studies are performed in an integral way neglecting variations of the gas composition, the use of pre-shaped particles (extrudates, shell-impregnation), or the change of the temperature over the catalyst bed. Only recently, it was shown that molecular information on a microscale is of importance also under *in situ* conditions, *e.g.*, during catalyst preparation [15,19–21] and in the catalytic reactor during operation [16,18,22].

Spatially resolved X-ray absorption spectroscopy is among other techniques such as micro XRD, micro infrared, micro UV–vis, and micro Raman spectroscopy a well suited tool for this purpose since it is element-specific and both amorphous and crystalline samples can be investigated [4,23–26]. Two different approaches have been reported: either the use of highly focused beams and scanning over the sample or the use of a two-dimensional position sensitive X-ray camera that allows recording X-ray images behind the sample. Nowadays, hard X-ray beams can be focused to less than 1 μm and information both in transmission and fluorescence can be obtained in this way on a micrometer scale [13,27–31]. Position

* Corresponding author. Tel.: +41 44 632 30 93; fax: +41 44 632 11 63.
E-mail address: grunwaldt@chem.ethz.ch (J.-D. Grunwaldt).
[1] Present address: Institut für Strukturphysik, TU Dresden, D-01062 Dresden, Germany.

0920-5861/$ – see front matter
doi:10.1016/j.cattod.2006.08.065

sensitive X-ray cameras can also give spatially resolved information [18,32]. In this case, the spatial resolution is on the 1–10 μm scale. For studying the structural changes over a catalyst bed, the use of a charged coupled device (CCD) camera compared to scanning with a microbeam has distinct advantages [18,32]: the absorption can be determined using the X-ray transmission images with and without sample and thus recording the absorption of the sample as function of the location (x, y) and energy E. This leads to a significantly faster measurement due to the parallel acquisition of the data points.

Recently, we observed a strong spatial change of the oxidation state of rhodium in Rh-based catalysts during the partial oxidation of methane [16,18]. Both a catalytic combustion and reforming (CCR) and a direct partial oxidation (DPO) mechanism have been proposed [33,34].

Catalytic combustion and reforming (CCR)

1. Combustion of methane:

$$CH_4 + 2O_2 \rightarrow CO_2 + 2H_2O, \qquad \Delta_r H = -801.7\,\mathrm{kJ/mol}.$$

2. Reforming of methane:

$$CH_4 + H_2O \rightarrow CO + 3H_2, \qquad \Delta_r H = 206.1\,\mathrm{kJ/mol}$$

$$CH_4 + CO_2 \rightarrow 2CO + 2H_2, \qquad \Delta_r H = 247.5\,\mathrm{kJ/mol}.$$

Direct partial oxidation of methane (DPO)

Partial oxidation of methane:

$$CH_4 + \tfrac{1}{2}O_2 \rightarrow CO + 2H_2, \qquad \Delta_r H = -35.5\,\mathrm{kJ/mol}.$$

From experimental and modelling studies [33–37], it is concluded that both the temperature and the flow (space velocity) influence the relative distribution of the gas composition during the catalytic partial oxidation of methane significantly. Hence, we investigated in this study the influence of both parameters on the structural composition of the catalyst in a fixed-bed. Moreover, if this technique is to be combined with tomography to obtain the three-dimensional distribution of the oxidation states inside a microreactor, the recording time required for a complete profile must be short. Therefore, ways to achieve this, such as reduced energy sampling or smaller energy intervals are also discussed in this contribution.

2. Experimental

The reaction was conducted using a 2.5 wt% Rh/Al_2O_3 catalyst in a quartz glass capillary microreactor (Markröhrchen, Hilgenberg GmbH, ca. 1 mm diameter, 20 μm wall thickness) as described in Ref. [38]. The *in situ* spectroscopic cell is similar to the one that has been originally proposed for *operando* XRD measurements [39,40] and was later used by a number of groups for *operando* EXAFS [38,41,42] even in fluorescence mode [43–45], SAXS [46] and even combined EXAFS/XRD [8] measurements. The 2.5 wt% Rh/Al_2O_3 catalyst was prepared by flame spray pyrolysis using a solution of Rh(III)acetylacetonate and aluminium-*sec*-butoxide in xylene sprayed in the flame (cf. Refs. [47,48]), which resulted in a high surface area and microcrystalline material (130 m^2/g determined by BET, Rh-particle size of 2–3 nm as evidenced by electron microscopy). Pre-mixed 6% CH_4/3% O_2/He was used as reaction gas and flows were controlled by mass flow controllers (Brooks, 0–50 ml/min). The outlet of the quartz glass microreactor was connected to a mass spectrometer (Balzers Thermostar). The microreactor was heated using an air blower with a controlled air flow regulated by a mass flow controller (Brooks, 0–2000 ml/min). The temperature of the heater was measured by a thermocouple (K-type) at the heating element (ring cartridge, SUVAG, Zurich, 300 W/230 V) in order to control a linear temperature ramp. The actual sample temperature was monitored just below the sample. The microreactor was additionally enclosed in a Kapton cap just above the heater where the hot air stream passed out of the oven. The whole assembly (*in situ* cell, heater) was mounted on a small stage (Huber, provided by HASYLAB) that allowed one to align the microreactor horizontally and vertically in the X-ray beam.

Spectroscopic information on the Rh-oxidation state was obtained in two ways. During dynamic changes of the reaction conditions (change in temperature, variation of the space velocity of the reaction mixture) the microreactor was scanned by an X-ray beam of 1 mm × 1 mm. By recording the intensities before and after the sample as a function of energy information on the oxidation state could be extracted from the XANES spectra at a spatial resolution of about 1 mm. After equilibration of the catalyst under the new experimental conditions more detailed spatially resolved X-ray absorption information from the reactor could be obtained by placing a two-dimensional position sensitive X-ray camera behind the reactor. A remote-controlled positioning system allowed us to move the camera in and out of the beam. In this way, either the camera or the ionization chamber I_1 behind the camera could be used for transmission measurements (Fig. 1). The setup has been described in more detail in Ref. [18]. In brief, the X-rays are converted in the detector into visible light in a thin single crystal scintillator that is imaged onto a CCD camera by a visible light microscope optic [49]. The effective pixel size is 3.5 μm. The energy was scanned in the XANES region around the Rh K-edge in steps of 1 or 2 eV (from 23190 to 23350 eV). At each energy E, an X-ray image was recorded with and without the capillary, effectively measuring the transmitted intensity $I_1(E, x, y)$ and incident intensity $I_0(E, x, y)$ in each pixel, where x and y denote the coordinates of the pixel. The exposure time for each image was 30 s. The reaction conditions of six selected investigations including the experimental parameters are summarized in Table 1. Obviously, we changed both the number of images and flat-fields and also the incoming intensity was varied by a different detuning of the monochromator crystal. The images were dark-field corrected, *i.e.*, the influence of the CCD dark current and read-out noise were removed by subtracting an averaged dark image (without X-rays) from each of the images. From the dark-field corrected transmission and flat-field images, the absorption along the

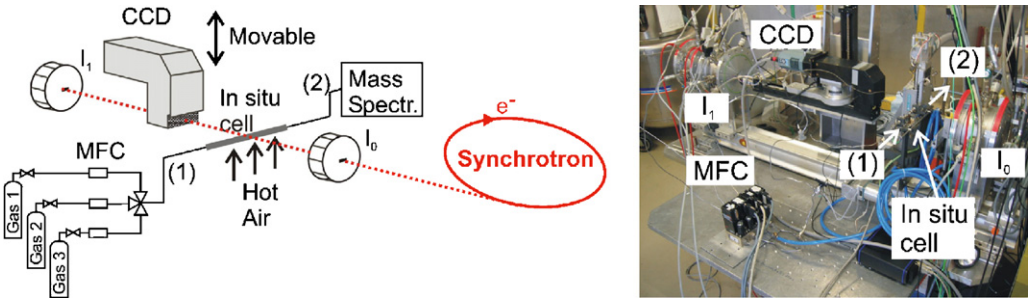

Fig. 1. Schematic setup and picture for mapping the oxidation state inside a catalytic reactor in two dimensions under reaction conditions; CCD-detector (position sensitive detection of the X-ray absorption), ionization chambers (''integral'' X-ray absorption spectra) as well as microreactor (*in situ* cell), oven and gas supply including MFCs (mass flow controllers) are depicted; (1) denotes the inlet of the *in situ* cell and (2) the outlet connected to a mass spectrometer.

Table 1
Parameters and reaction conditions during the different scans for 2D-profiling (details, cf. experimental part)

Scan number	Position of the centre (mm)	Temperature (°C)	Flow (ml/min)	Detuning of I_0 (%)	Number of images and flat-fields	Recording time (min)
1	1.8	352	12.5	7	160 with $\Delta E = 1$ eV	160
2	1.8	362	12.5	70	160 with $\Delta E = 1$ eV	160
3	1.5	378	12.5	70	160 with $\Delta E = 1$ eV	160
4	6.0	338	12.5	70	80 with $\Delta E = 2$ eV	90
5	6.5	338	20	70	80 with $\Delta E = 2$ eV	90
6	1.5	344	25	70	80 with $\Delta E = 2$ eV	90

optical axis is obtained for each pixel. Further information on the experimental procedure is given in Ref. [18].

The experiments were performed at beamline X1 at HASYLAB (DESY, Hamburg), using a Si(3 1 1) double crystal monochromator. The second crystal was typically detuned to 70% of the maximum intensity in order to remove higher harmonics. The X-ray beam was slit down to 1 mm × 1 mm for scanning along the microreactor and the incoming intensity I_0 and the transmitted intensity I_1 were determined using ionization chambers filled with 100 and 400 mbar Kr, respectively. The scans were taken in the step scanning mode between 23180 and 23310 eV and background subtraction was performed using the WINXAS 3.0 software [50]. When using the CCD camera, the X-ray slits were set to 3 mm × 1.5 mm. Processing the data including the calculation of the distribution of oxidized and reduced Rh-species was performed using software developed in-house. For this purpose spectra characteristic for oxidized and reduced rhodium species were fitted together with the featureless component for uncharacteristic absorption to the measured spectra at each pixel.

3. Results

3.1. Temperature dependence of axial changes of the Rh-oxidation state inside the catalyst bed monitored by 1D-scanning

In a first experiment, 14.5 mg of 2.5 wt% Rh/Al_2O_3 were loaded in the microreactor and heated to 352 °C in 6% CH_4/3% O_2/He. At 300 °C carbon dioxide and water production was detected by the mass spectrometer and around 340 °C carbon monoxide and hydrogen were formed while oxygen disappeared. At 352 °C, no oxygen was observed anymore at the outlet of the microreactor (cf. entry 2 in Table 2). Hydrogen,

Table 2
On-line mass spectrometric analysis of methane (*m/e* = 15), oxygen (*m/e* = 32), water (*m/e* = 18), carbon dioxide (*m/e* = 44), hydrogen (*m/e* = 2), and trace *m/e* = 28 which stems both from CO and CO_2 under different static reaction conditions at the outlet of the microreactor cell (temperature measured at the outer wall of the microreactor; flow 12.5 ml/min; 14.5 mg of 2.5% Rh/Al_2O_3; all values are given in relative units)

Experiment no.	Temperature (°C)	*m/e* = 15	*m/e* = 32	*m/e* = 18	*m/e* = 44	*m/e* = 2	*m/e* = 28
1	RT	0.4	1.2	0.02	0	0	0.01
2	352	0.28	0	1.7	1.9	2.2	0.23
3	362	0.26	0	1.5	1.5	2.7	0.32
4	378	0.24	0	1.4	1.4	3.1	0.30
5	300	0.32	0.67	1.6	1.0	0.08[a]	0.19
6	331	0.29	0.01	1.6	1.5	0.9	0.26
7	338	0.29	0	1.6	1.5	1.5	0.26
8	338[b]	0.29	0	1.5	1.4	1.2	0.23

[a] Further decreasing during measuring.
[b] After increase of gas flow from 12.5 to 20 ml/min.

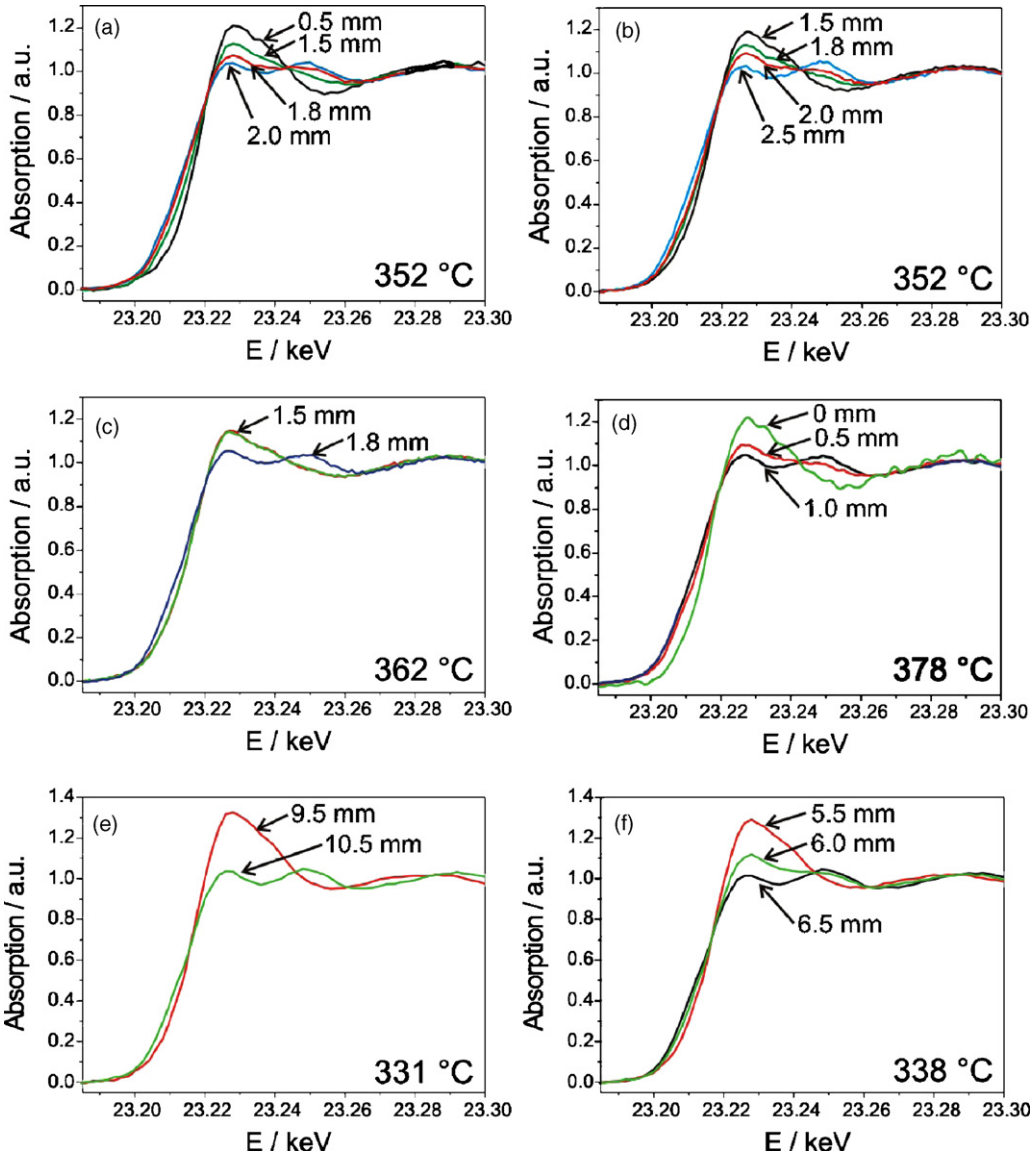

Fig. 2. XANES spectra taken with a 1 mm × 1 mm X-ray beam at different temperatures and positions inside the fixed-bed: (a) 352 °C (after 30 min equilibration time); (b) 352 °C (after 7 h equilibration time); (c) 362 °C; (d) 378 °C; (e) 331 °C; (f) 338 °C.

carbon monoxide, carbon dioxide and methane were detected above this temperature.

Scanning along the microreactor showed that a steep gradient in the oxidation state established along the axial direction of the capillary. At 352 °C, the gradient occurred at about 2 mm behind the inlet of the catalytic reactor[2] (see Fig. 2a). As Fig. 2b shows, the gradient was stable over a period of several hours, but a certain equilibration time was required for its establishment. Increasing the temperature to 362 °C and 378 °C shifted the gradient zone to 1.5 mm and <0.5 mm (Fig. 2c and d), respectively. The selectivity and activity towards hydrogen and carbon monoxide increased significantly upon increase of the temperature (entries 2 and 3 in Table 2; note that the MS-traces are not calibrated).

Several features such as the rather steep structural variations in the catalyst bed, the strong changes in the catalytic activity, and the results presented in Fig. 2d already demonstrate the limitation of scanning with a rather large beam of 1 mm × 1 mm: on the one hand more accurate information on the changes in the catalyst bed is required, on the other hand probing at the axial position "0" in the catalyst bed implies that only half of the X-ray beam hits the catalyst bed and more accurate scanning with a smaller beam would be desirable. Due to by-passing of the X-ray beam, the spectrum at "0" mm is also more noisy (spectrum was smoothed) than the ones at position 0.5 or 1 mm, respectively.

As expected, cooling down to 331 °C resulted in a shift of the gradient towards the end of the microreactor, located at about 10 mm of the ca. 15 mm long catalyst bed (Fig. 2e).

[2] Note that the position "2 mm" behind the inlet of the catalytic reactor denotes that the centre of the X-ray beam hits the sample 2 mm behind the start of the catalytic bed thus probing the region from 1.5 to 2.5 mm in this case.

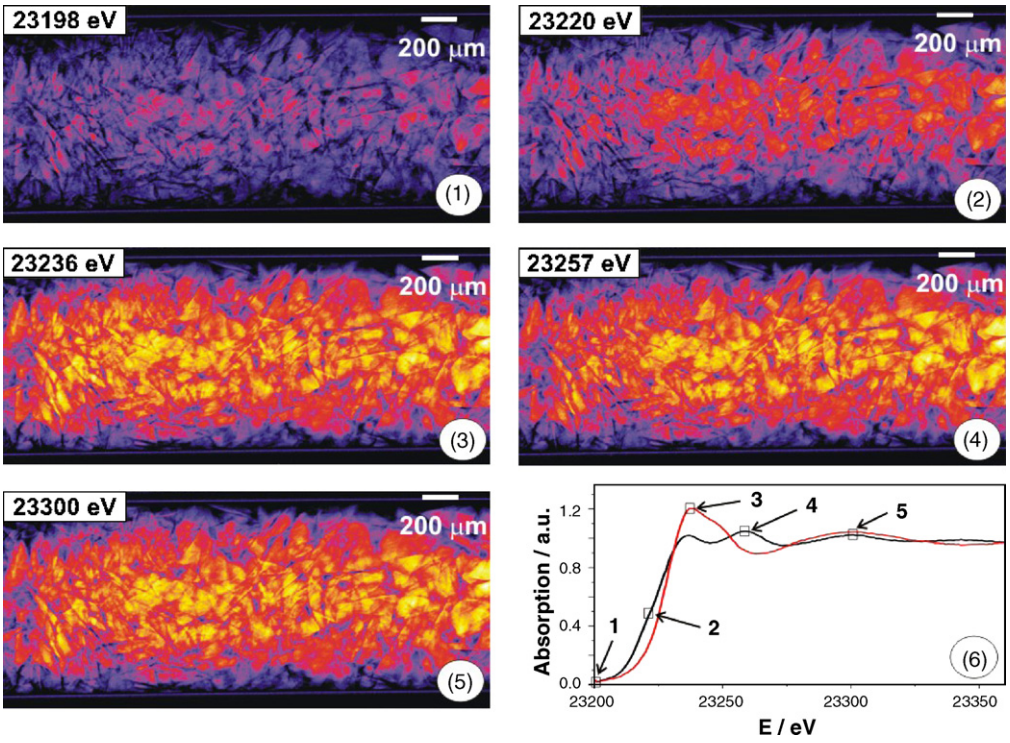

Fig. 3. Absorption extracted from transmission images (recorded by the CCD camera; flat- and dark-field corrected) of Rh/Al_2O_3 inside the microreactor at 362 °C during the CPO of methane at the energies indicated in the corresponding images; centre position is 1.8 mm for image (1)–(5); (6) shows the extracted XANES spectra from the flat- and dark-field corrected transmission images at about 0.3 and 3.3 mm at 362 °C.

Also the selectivity towards hydrogen and carbon monoxide decreased (entry 6 in Table 2). Note that a too strong temperature decrease led to an extinction of the reaction (observed at 300 °C, cf. entry 5 in Table 2). This resulted in an oxidation of the Rh-species along the whole catalyst bed. At a slight temperature increase from 330 to 338 °C the gradient zone was instead shifted to 6 mm (Fig. 2f). Within the accuracy of the local probing technique the gradient zone was reproducible. Also the catalytic performance was similar.

3.2. 2D-monitoring of structural changes occurring in the catalyst bed using a CCD camera

Fig. 3 depicts selected flat- and dark-field corrected transmission images at 362 °C, corresponding to the 1D-scan in Fig. 2c. Five characteristic energies were selected as marked in the XANES spectra of Fig. 3, which were extracted at position 0.3 and 3.3 mm in the catalyst bed. The centre position was the same as during the 1D-scan in Fig. 2c. Below the Rh K-edge (Fig. 3(1), 23198 eV) the absorption is significantly

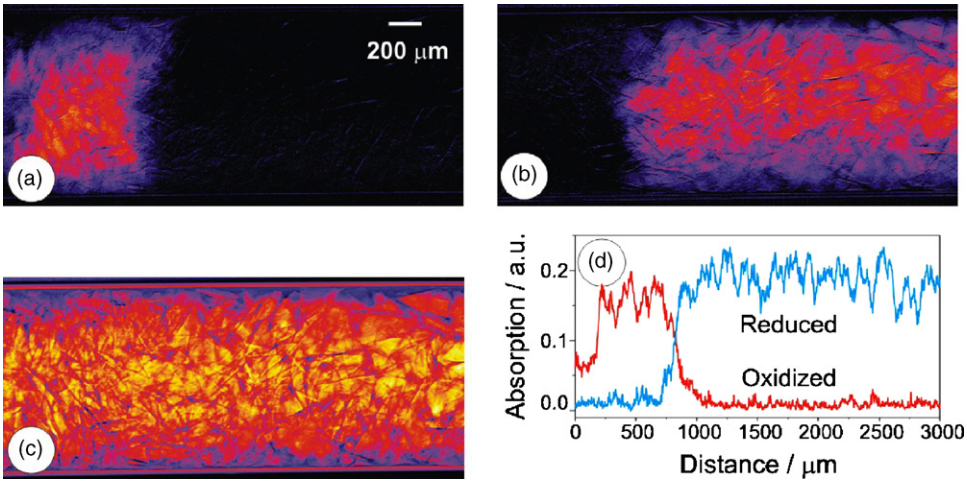

Fig. 4. Extracted components from the analysis of the 160 dark- and flat-field corrected transmission images: (a) oxidized Rh-species; (b) reduced Rh-species; (c) featureless background; (d) relative concentration of the oxidized (red) and reduced (blue) Rh-particles in the axis of the fixed-bed (conditions: 362 °C, space velocity $1.9 \times 10^5\ h^{-1}$). (For interpretation of the references to colour in this figure legend, the reader is referred to the web version of the article.)

smaller than above the Rh K-edge (Fig. 3(3–5)) and due to the strong whiteline of Rh in oxidized state (23236 eV), the absorption is higher at the inlet of the microreactor. In this case altogether 360 images, at each energy one with and one without the microreactor, were recorded with the CCD camera resulting in 160 flat- and dark-field corrected transmission images of the Rh/Al_2O_3 catalyst inside the microreactor (available as movie in the support information). These images contain the complete spectral information for determining the distribution of oxidized and reduced Rh-species inside the microreactor (for details on the mathematical transformation and description of the procedure, cf. experimental part and Ref. [18]). The results are depicted in Fig. 4.

Operando spectroscopic studies require that the data can be extracted in a reasonable time interval. The scan shown in Fig. 4 was recorded during 160 min (Table 1) using 1 eV steps. Fig. 5 shows what would happen if the images were taken in larger energy steps, in a smaller energy range around the absorption edge, and at a few selected energies. Obviously, still the same information would be gained. However, the resolution decreases slightly. This reduction in resolution is probably due to a reduced sampling of the XANES features and an overall reduction in counting statistics, a similar effect as observed if the scans were recorded with lower intensity (see later). Selecting only five marked points, as, *e.g.*, shown in Fig. 3(6), did not result in a sufficient signal-to-noise ratio. Obviously XANES spectra around the Rh K-edge are required, underscoring the importance of taking images in the entire XANES region.

Another important issue is the intensity of the incoming beam and/or the exposure time. Fig. 6 shows that this has in fact a strong influence. In the first row (Fig. 6a) the images were taken with 1/10 of the intensity of the beam by detuning to 7% instead of 70% compared to the other images at other temperatures (cf. Table 1, Fig. 6b–d). Since the resolution is worse at lower beam intensity, it can be expected that the resolution will improve at insertion devices with higher X-ray beam intensity. Moreover, the whole experiment will be speeded up in this case.

Fig. 6 also shows variations of the structure in the catalyst bed as a function of temperature. In agreement with the results in Fig. 2, the gradient shifts towards the inlet of the microreactor. By increasing the temperature from 352 to 362 °C, the gradient is shifted by 500 μm towards the inlet and another 600 μm by further increase to 378 °C (200–300 μm behind the entrance of the catalyst bed). With the help of the flat- and dark-field corrected images (on the left in Fig. 6) one can align the different snapshots within better than 10 μm. Note the slightly conical shape of the oxidation state distribution in the gradient zone. While at these relatively high temperatures

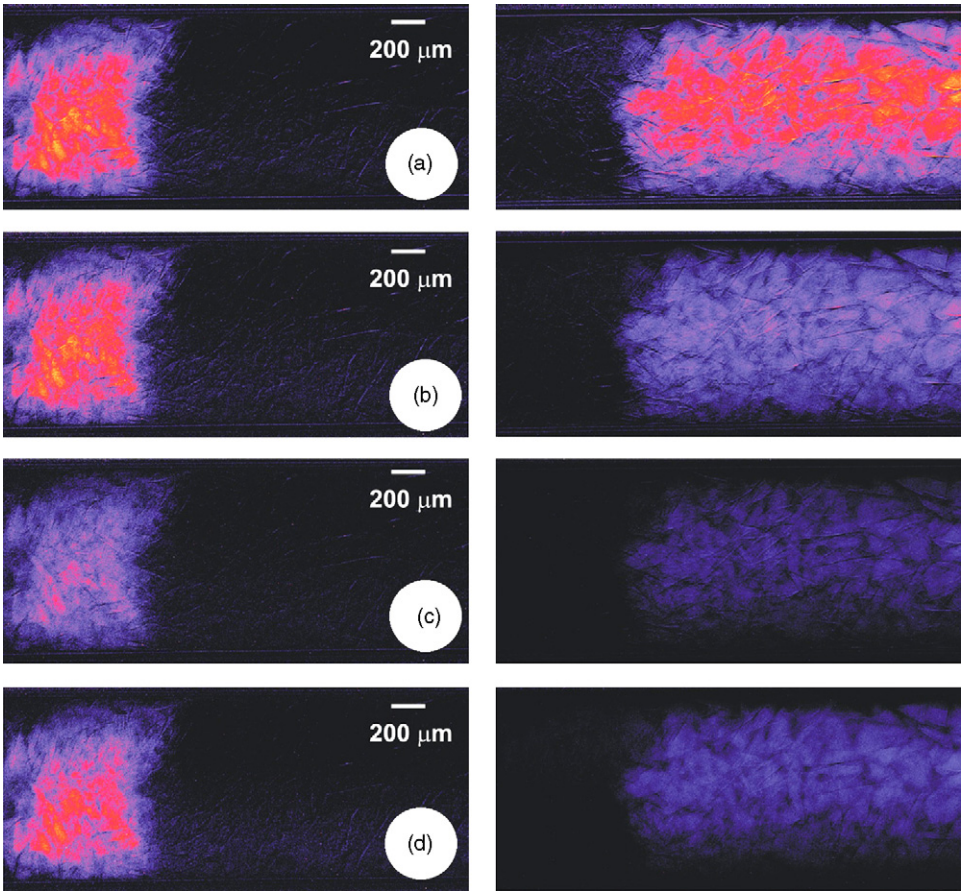

Fig. 5. Effect on the distribution of oxidized and reduced Rh-particles when changing the number of images from (a) 160 (1 eV steps, from 23190 to 23350 eV) to (b) 80 (2 eV steps, same energy interval), (c) 40 (4 eV steps, same energy interval) and (d) 40 (2 eV steps, from 23190 to 23270 eV).

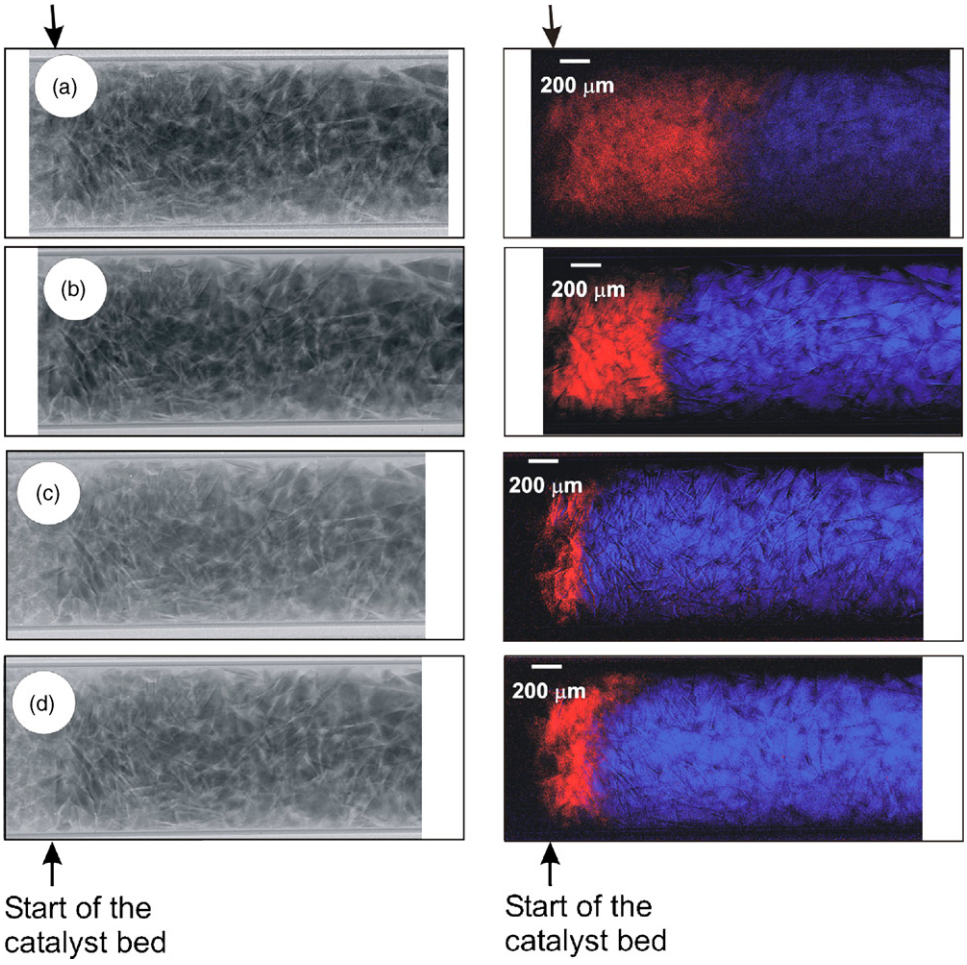

Fig. 6. Flat- and dark-field corrected images and amount of oxidized and reduced Rh-species at (a) 352 °C; (b) 362 °C, (c) 378 °C and (d) 344 °C (space velocity doubled to $3.8 \times 10^5\ h^{-1}$); axial position of the entrance of the catalyst bed is indicated.

the change in the position of the gradient zone is only several 100 μm the change in the gradient location is more significant when the temperature is lowered to 331 or 338 °C. Fig. 7b represents the results at 338 °C. The gradient zone is located at 5.8 mm behind the entrance of the catalyst bed. Interestingly, in that case the conical shape is also less pronounced. In addition, the conversion to hydrogen and carbon monoxide is lower than at 352 °C (cf. Table 2).

3.3. Axial change of the Rh-oxidation state in the catalyst bed monitored during change of the space velocity

The influence of different space velocities on the Rh-oxidation state was studied at two different temperatures (338 and 344 °C). In Figs. 8 and 9, results from 1D-scans along the axis of the catalyst bed are shown for the two different temperatures. Obviously, at 338 °C the gradient moves towards the outlet of the reactor when increasing the space velocity from $1.9 \times 10^5\ h^{-1}$ ($12.5\ ml\ min^{-1}$) to $3.8 \times 10^5\ h^{-1}$ ($25\ ml\ min^{-1}$). As expected, changes in the space velocity were reflected in the catalytic performance as well, *i.e.*, the yield of hydrogen and carbon monoxide decreased (cf. Table 2). However, at a higher temperature (344 °C) an opposite effect was observed. In this case, the gradient zone moved towards the inlet of the reactor. This is also supported by the 2D-images of the Rh^{3+}/Rh^0 distribution in the catalyst bed. At 338 °C, the gradient zone moved by 750 μm towards the outlet (Fig. 7), whereas at 344 °C the gradient zone was shifted by 925 μm towards the inlet of the microreactor compared to the experiment at lower flow at 352 °C (Figs. 3a and 3d). This striking result may be explained by self-heating of the catalyst due to faster exothermic reactions and axial heat conduction which shift the gradient towards the inlet of the microreactor. At lower temperatures the gradient is shifted towards the end of the catalyst bed because the reaction rate is smaller and more methane/oxygen need to be consumed by the total combustion before in the downstream part of the reactor the reforming reaction leads to H_2 and CO-formation.

4. Discussion

The importance of determining structural information on a molecular level as a function of the position inside a catalytic reactor under *in situ* conditions has been demonstrated in the case of the partial oxidation of methane over Rh/Al_2O_3. Preferentially, such studies could be performed in real catalytic reactors determining gas and catalyst composition as function

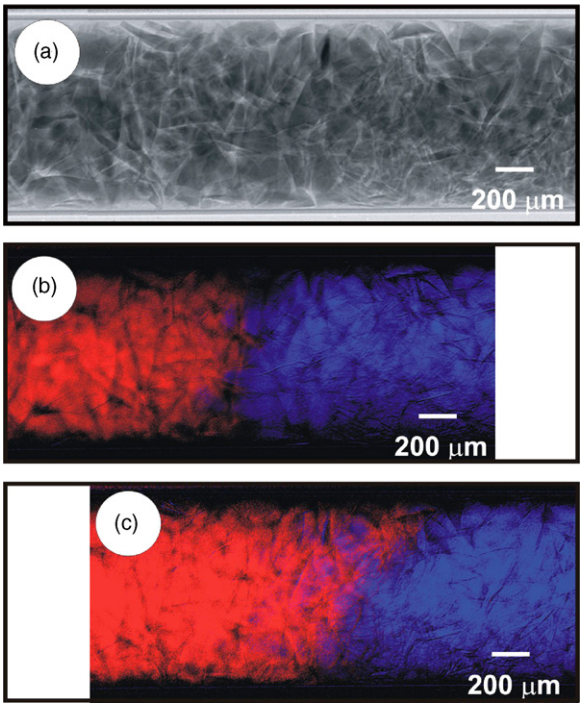

Fig. 7. Structural changes over the catalyst bed due to variation of the space velocity at 338 °C: (a) flat- and dark-field corrected image of catalyst bed; (b) amount of oxidized (red) and reduced (blue) at 338 °C (space velocity $1.9 \times 10^5\ h^{-1}$); (c) 338 °C (space velocity $3.8 \times 10^5\ h^{-1}$). (For interpretation of the references to colour in this figure legend, the reader is referred to the web version of the article.)

of the location in the reactor. Here, we simplified the situation by performing the studies in a microreactor amenable for transmission X-ray absorption spectroscopy. The structure was measured either by an X-ray beam of 1 mm × 1 mm or a position sensitive X-ray camera which results in an effective spatial resolution of about 20 μm. The two modes were combined as depicted in Fig. 1.

Due to parallel data acquisition in an area of 3 mm × 1.5 mm *in situ* studies were possible also during 2D-mapping inside a microreactor. At second generation synchrotron radiation sources, the acquisition time of one profile of the Rh^{3+}/Rh^0 distribution inside the microreactor is limited to about 1 h, but the strong influence of the intensity (Fig. 6) evidences that the signal-to-noise ratio will significantly improve at a higher flux. The lower time frame for spectroscopic profiling will therefore mainly be limited to the movement of the detector and the microreactor, particularly since CCD-based systems for time-resolved experiments for the subsecond region have already been developed [49,51–53]. This will also allow to combine this technique with tomography. Fig. 5 also shows that advantageously a full XANES spectrum is taken at each location leading to a better resolved distribution of the Rh-species inside the catalyst bed. Selected points as, *e.g.*, depicted in Fig. 3(6) are not sufficient to determine the concentration of Rh^{3+}- and Rh^0-species inside the catalyst bed.

The gradient inside the microreactor changed in a characteristic way both as function of temperature and gas

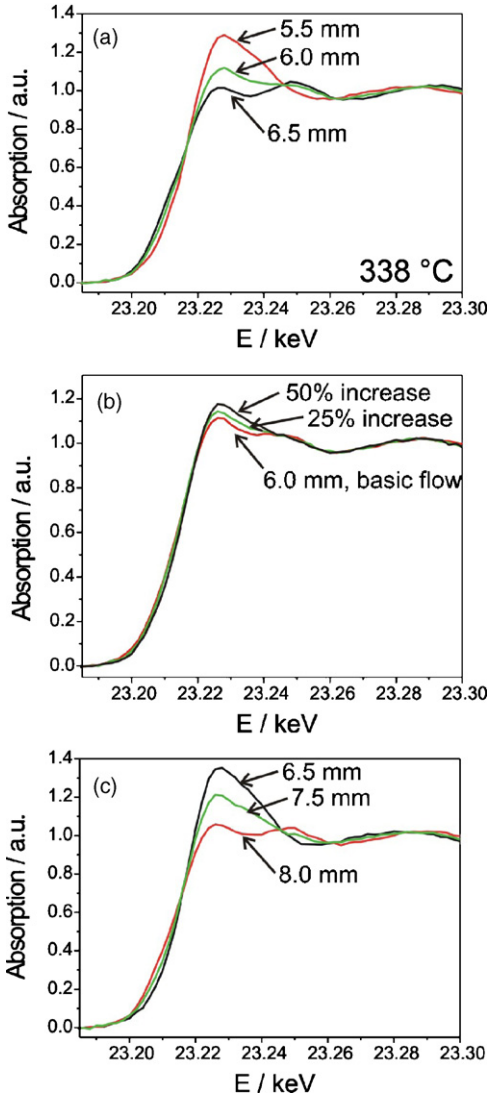

Fig. 8. XANES spectra taken with a 1 mm × 1 mm X-ray beam at 338 °C and changed flow conditions: (a) 12.5 ml/min; (b) during increase to 20 ml/min; (c) 20 ml/min.

flow. Below the ignition temperature of the partial oxidation reaction, rhodium was mainly in oxidized state, even if the catalytic combustion of methane to carbon dioxide and water was already detected by the mass spectrometer. Above the ignition temperature of the partial methane oxidation reaction, the amount of hydrogen and carbon monoxide produced correlated with the position of the gradient inside the microreactor: the gradient was shifted towards the inlet of the microreactor when the selectivity towards hydrogen and carbon monoxide increased. Both a catalytic combustion and reforming mechanism and a direct partial oxidation mechanism were reported in literature [33,34]. Obviously, as long as Rh remains in oxidized state, methane is totally combusted. The appearance of the formation of hydrogen and carbon monoxide concomitant with metallic-like rhodium in the downstream part of the reactor could indicate a CCR mechanism at these temperatures, which dominates towards the reactor outlet. However, another possibility is that the DPO mechanism is only effective at higher temperatures. In line with our observation,

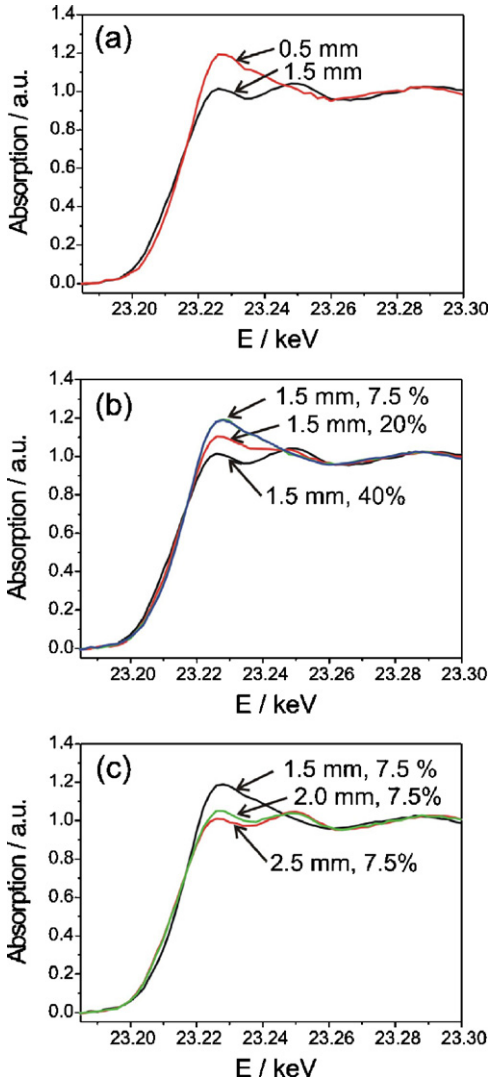

Fig. 9. XANES spectra taken with a 1 mm × 1 mm X-ray beam at 344 °C and changed flow conditions: (a) 25 ml/min; (b) during decrease to 5 ml/min; (c) 5 ml/min.

Hu and Ruckenstein conclude that at lower temperatures combustion and reforming are often prevalent [34]. At higher temperatures, we also found a significantly higher selectivity towards hydrogen and carbon monoxide on the present Rh/Al_2O_3 catalyst (not shown).

Strikingly different effects of the space velocity were observed at the two temperatures investigated: at lower temperature the gradient is generally shifted towards the outlet if the space velocity is increased (Figs. 7 and 8). In contrast, at higher temperature the opposite was observed (Figs. 6 and 9), probably due to self-heating and heat conduction in the catalyst bed as described in various studies before [33,35–37,54,55]. This self-heating of the catalyst bed is also indicated by the different shape of the gradient that is more conical at higher temperatures. In future, a combination of the experiment with an IR-camera to determine the temperature inside the catalyst bed will therefore be advantageous. This would also provide the opportunity to compare the data to modelling studies, *e.g.*, reported in Ref. [37].

5. Conclusions and outlook

Our study illustrates that in a fixed-bed catalytic reactor prominent temperature and concentration gradients can result in a dramatic spatial variation of the catalyst structure, indicating the need for spatially resolved *in situ* (or *operando*) spectroscopy. X-ray absorption spectroscopy is shown to be a well-suited tool for detecting such variations and to give additional insight into the mechanism. XAS can provide information on the structure (oxidation state, geometry and nearest neighbors) and is complementary to the recently applied techniques micro UV–vis, micro Raman, micro XRD, micro XRF, and magnetic resonance imaging. Parallelization as by the use of a CCD camera or rapid scanning (QEXAFS, DEXAFS) in combination with a focused beam are however required during *in situ* studies. The application of a CCD camera for X-ray detection or the use of a microfocussed beam will strongly depend on the scientific question to be addressed. For mapping of the oxidation state, as in the present case, or the coordination geometry with characteristic changes in the pre-edge region (*e.g.*, octahedral and tetrahedral titanium, cf. Ref. [56]), the acquisition of XANES spectra is sufficient and thus the approach using a CCD or even a Fast Readout Low Noise (FReLoN, cf. [57]) CCD camera is very attractive. However, in other cases the whole EXAFS spectrum needs to be recorded. In those studies scanning of selected parts with a micrometer focused beam may be advantageous.

In future, it will be interesting to extend such studies from 2D-mapping to tomography as shown *ex situ* on a Cu/ZnO catalyst using a combination of microfocussing and QEXAFS [13]. Furthermore a better focusing, higher X-ray beam intensity and CCD or FReLoN cameras with better resolution will enhance both spatial and time resolution. The present study as well as studies by micro UV–vis, micro Raman and magnetic resonance imaging show the need for spatially resolved spectroscopy in catalysis: spatial variations can occur during catalyst preparation/impregnation [15,19–21] and in a catalytic reactor during activation and/or reaction, and can embrace catalyst structure, fluid dynamics and temperature [16,18,22,58]. In the latter case, structural studies should be preferentially combined with the local detection of temperature and performance of the catalysts. Better understanding of both preparation of catalysts and the structural evolution of active sites under reaction conditions will be beneficial to the development of new catalysts and catalyst optimization. Spatially resolved spectroscopy will also be interesting for all other fields where spatial variations of chemical and structural properties are affecting the functionality of materials.

Support information

A movie showing all flat- and dark-field corrected transmission images from 23190 to 23350 eV in 1 eV steps can be received from the author as electronic support information.

Acknowledgements

The authors thank ETH Zurich and the Swiss Commission for Technology and Innovation (CTI, TopNano 21 grants 5978.2 TNS and 6740.1 TNS) for financial support. HASYLAB (beamline X1, DESY, Hamburg) is gratefully acknowledged for granting beamtime and Mathias Herrmann (HASYLAB) and Bernd Reime (HASYLAB) for their help during the measurements.

References

[1] G.A. Somorjai, J.M. Thomas (Eds.), Top. Catal. 8 (1999).
[2] H. Topsøe, J. Catal. 216 (2003) 155.
[3] J.M. Thomas, Angew. Chem. Int. Ed. 38 (1999) 3588.
[4] J.-D. Grunwaldt, B.S. Clausen, Top. Catal. 18 (2002) 37.
[5] B.M. Weckhuysen, Chem. Commun. (2002) 97.
[6] M.A. Banares, Catal. Today 100 (2005) 71.
[7] B.M. Weckhuysen, In-situ Spectroscopy of Catalysts, American Scientific Publishers, Stevenson Ranch, California, 2004.
[8] J.-D. Grunwaldt, A.M. Molenbroek, N.-Y. Topsøe, H. Topsøe, B.S. Clausen, J. Catal. 194 (2000) 452.
[9] P.L. Hansen, J.B. Wagner, S. Helveg, J.R. Rostrup-Nielsen, B.S. Clausen, H. Topsøe, Science 295 (2002) 2053.
[10] S. Helveg, C. Lopez-Cartes, J. Sehested, P.L. Hansen, B.S. Clausen, J.R. Rostrup-Nielsen, F. Abild-Pedersen, J.K. Nørskov, Nature 427 (2004) 426.
[11] R. Fernandez-Ruiz, M. Furio, F.C. Galisteo, C. Larese, M.L. Granados, R. Mariscal, J.L.G. Fierro, Anal. Chem. 74 (2002) 5463.
[12] P. Lucena, J.M. Vadillo, J.J. Laserna, Appl. Spectr. 55 (2001) 267.
[13] C.G. Schroer, M. Kuhlmann, T.F. Günzler, B. Lengeler, M. Richwin, B. Griesebock, D. Lützenkirchen-Hecht, R. Frahm, E. Ziegler, A. Mashayekhi, D.R. Haeffner, J.-D. Grunwaldt, A. Baiker, Appl. Phys. Lett. 82 (2003) 3360.
[14] M. Moldovan, S. Rauch, G.M. Morrison, M. Gomez, M.A. Palacios, Surf. Interface Anal. 35 (2003) 354.
[15] J.A. Bergwerff, T. Visser, J.R.G. Leliveld, B.D. Rossenaar, K.P.d. Jong, B.M. Weckhuysen, J. Am. Chem. Soc. 126 (2004) 14548.
[16] J.-D. Grunwaldt, A. Baiker, Catal. Lett. 99 (2005) 5.
[17] J.A. Bergwerff, L.G.A. van de Water, T. Visser, P. de Peinder, B.R.G. Leliveld, K.P. de Jong, B.M. Weckhuysen, Chem. Eur. J. 11 (2005) 4592.
[18] J.-D. Grunwaldt, S. Hannemann, C.G. Schroer, A. Baiker, J. Phys. Chem. B 110 (2006) 8674.
[19] A. Baiker, W.L. Holstein, J. Catal. 84 (1983) 178.
[20] A.A. Lysova, I.V. Koptyug, R.Z. Sagdeev, V.N. Parmon, J.A. Bergwerff, B.M. Weckhuysen, J. Am. Chem. Soc. 127 (2005) 11916.
[21] L.G. van de Water, J.A. Bergwerff, T.A. Nijhuis, K.P. de Jong, B.M. Weckhuysen, J. Am. Chem. Soc. 127 (2005) 5024.
[22] I.V. Koptyug, A.A. Lysova, R.Z. Sagdeev, V.A. Kirillov, A.V. Kulikov, V.N. Parmon, Catal. Today 105 (2005) 464.
[23] Y. Iwasawa, X-ray Absorption Fine Structure for Catalysts and Surfaces, vol. 2, World Scientific, Singapore, 1996.
[24] B.S. Clausen, Catal. Today 39 (1998) 293.
[25] M.A. Newton, A.J. Dent, J. Evans, Chem. Soc. Rev. 32 (2002) 83.
[26] J.D. Grunwaldt, A. Baiker, Phys. Chem. Chem. Phys. 7 (2005) 3526.
[27] B. Lengeler, C. Schroer, J. Tümmler, B. Benner, M. Richwin, A. Snigirev, I. Snigireva, M. Drakopoulos, J. Synchrotron Radiat. 6 (1999) 1153.
[28] P.M. Bertsch, D.B. Hunter, Chem. Rev. 101 (2001) 1809.
[29] K. Proost, L. Vincze, K. Janssens, N. Gao, E. Bulska, M. Schreiner, G. Falkenberg, X-ray Spectrom. 32 (2003) 215.
[30] D. Vantelon, A. Lanzirotti, A.C. Scheinost, R. Kretzschmar, Environ. Sci. Technol. 39 (2005) 4808.
[31] M. Vespa, R. Dähn, D. Grolimund, M. Harfouche, E. Wieland, A.M. Scheidegger, J. Geochem. Explor. 88 (2006) 77.
[32] C. Rau, A. Somogyi, A. Simionovici, Nucl. Instrum. Methods Phys. Res. B 203 (2003) 444.
[33] A.P.E. York, T.C. Xiao, M.L.H. Green, Top. Catal. 22 (2003) 345.
[34] Y.H. Hu, E. Ruckenstein, Adv. Catal. 48 (2004) 297.
[35] D.A. Hickman, L.D. Schmidt, Science 259 (1993) 343.
[36] D.A. Hickmann, L.D. Schmidt, React. Kinet. Catal. 39 (1993) 1164.
[37] R. Schwiedernoch, S. Tischer, C. Correa, O. Deutschmann, Chem. Eng. Sci. 58 (2003) 633.
[38] J.-D. Grunwaldt, M. Caravati, S. Hannemann, A. Baiker, Phys. Chem. Chem. Phys. 6 (2004) 3037.
[39] B.S. Clausen, G. Steffensen, B. Fabius, J. Villadsen, R. Feidenhans'l, H. Topsøe, J. Catal. 132 (1991) 524.
[40] G. Sankar, J.M. Thomas, F. Rey, G.N. Greaves, Chem. Commun. (1995) 2549.
[41] B.S. Clausen, L. Gråbæk, G. Steffensen, P.L. Hansen, H. Topsøe, Catal. Lett. 20 (1993) 23.
[42] G. Meitzner, S.R. Bare, H. Woo, D.A. Fischer, Rev. Sci. Instrum. 69 (1998) 2618.
[43] P. Kappen, J.-D. Grunwaldt, B.S. Hammershøi, L. Tröger, G. Materlik, B.S. Clausen, J. Catal. 198 (2001) 56.
[44] J.-D. Grunwaldt, P. Kappen, B.S. Hammershøj, L. Tröger, B.S. Clausen, J. Synchrotron Radiat. 8 (2001) 572.
[45] J.-D. Grunwaldt, S. Hannemann, J. Göttlicher, S. Mangold, M.A. Denecke, A. Baiker, Phys. Scr. T115 (2005) 760.
[46] J.W. Andreasen, O. Rasmussen, R. Feidenhans'l, F.B. Rasmussen, R. Christensen, A.M. Molenbroek, G. Goerigk, J. Appl. Cryst. 36 (2003) 812.
[47] W.J. Stark, S.E. Pratsinis, A. Baiker, Chimia 56 (2002) 485.
[48] R. Strobel, J.-D. Grunwaldt, A. Camenzind, S.E. Pratsinis, A. Baiker, Catal. Lett. 104 (2005) 9.
[49] A. Koch, C. Raven, P. Spanne, A. Snigirev, J. Opt. Soc. Am. A 15 (1998) 1940.
[50] T. Ressler, J. Synchrotron Radiat. 5 (1998) 118.
[51] Y.X. Wang, F. de Carlo, D.C. Mancini, I. McNulty, B. Tieman, J. Bresnahan, I. Foster, J. Insley, P. Lane, G. von Laszewski, C. Kesselman, M.H. Su, M. Thiebaux, Rev. Sci. Instrum. 72 (2001) 2062.
[52] N. Yagi, K. Inoue, T. Oka, J. Synchrotron Radiat. 11 (2004) 456.
[53] M.D. Michiel, J.M. Merino, D. Fernandez-Carreiras, T. Buslaps, V. Honkimäki, P. Falus, T. Martins, O. Svensson, Rev. Sci. Instrum. 76 (2005) 043702.
[54] B. Li, K. Maruyama, M. Nurunnabi, K. Kunimori, K. Tomishige, Ind. Eng. Chem. Res. 44 (2005) 485.
[55] F. Basile, G. Fornasari, F. Trifirò, A. Vaccari, Catal. Today 64 (2001) 21.
[56] J.-D. Grunwaldt, C. Beck, W.J. Stark, T. Mallat, A. Hagen, A. Baiker, Phys. Chem. Chem. Phys. 4 (2002) 3514.
[57] A. Bravin, S. Fiedler, P. Coan, J.-C. Labiche, C. Ponchut, A. Peterzol, W. Thomlinson, Nucl. Instrum. Methods Phys. Res. A 510 (2003) 35.
[58] E.H.L. Yuen, A.J. Sederman, L.F. Gladden, Appl. Catal. A 232 (2002) 29.